



Microstructure and mechanical properties of TiC-Fe surface gradient coating on a pure titanium substrate prepared in situ

Haiqiang Bai^{a, c}, Lisheng Zhong^{a, b, *}, Zhao Shang^a, Yunhua Xu^{a, b, c, **}, Hong Wu^b, Jiaming Bai^a, Yingchun Ding^{a, d}

^a School of Material Science and Engineering, Xi'an University of Technology, Xi'an, 710048, PR China

^b Shaanxi Key Laboratory of Nano Materials and Technology, Xi'an, 710048, China

^c School of Chemistry and Chemical Engineering, Yulin University, Yulin, 719000, China

^d College of Optoelectronics Technology, Chengdu University of Information Technology, Chengdu, 610225, China

ARTICLE INFO

Article history:

Received 25 April 2018

Received in revised form

29 August 2018

Accepted 30 August 2018

Available online 1 September 2018

Keywords:

In situ reaction

TiC-Fe surface gradient coating

Microstructure

Mechanical properties

ABSTRACT

A TiC-Fe surface gradient coating was prepared on the surface of pure titanium by a simple two-step heat-treatment process ($1150\text{ }^{\circ}\text{C} \times 5\text{ min} + 1000\text{ }^{\circ}\text{C} \times 10\text{ h}$). The phase composition, microstructure, nanoindentation hardness, elastic modulus, fracture toughness, and adhesion strength of the TiC-Fe surface gradient coating were investigated using X-ray diffraction (XRD), scanning electron microscopy (SEM), electron backscattered diffraction (EBSD), nanoindentation testing, and scratch testing. The results reveal that the TiC-Fe surface gradient coating was composed of dense TiC grains and a small amount of α -Fe. The TiC-Fe surface gradient coating was divided into three zones according to the variation in the volume fractions of TiC particulate and α -Fe phase. These zones were labeled as follows: a columnar TiC zone (I zone), a large particle TiC zone (II zone) and a large bulk TiC zone (III zone). The formation process and mechanism of the TiC-Fe surface gradient coating include the nucleation growth of TiC grains, followed by diffusion and in situ reactions between titanium and carbon. The nanoindentation hardness and elastic modulus for cross section of the TiC-Fe surface gradient coating ranged from 19.1 to 31.7 GPa and from 368.1 to 464.3 GPa, respectively. The fracture toughness values of I zone, II zone and III zone are 3.5, 1.6 and 3.1 MPa $\text{m}^{1/2}$, respectively, and these values largely depend on composition and microstructure. Investigations of crack surface morphologies indicate that radial cracks at the corners of the indentation originate from the crossing of slip bands and that the toughening mechanism was mainly crack deflection and bridging. In addition, the scratch testing indicated that the coating exhibited excellent coating/substrate adhesion strength.

© 2018 Elsevier B.V. All rights reserved.

1. Introduction

Hard coatings play an important role in industrial applications to improve the wear resistance and strength of engineered components and prolonging their service lifetimes. Transition metal carbides, nitrides and borides are widely used as hard coating materials because of their high hardness, high melting point, and good electrical and thermal conductivities [1–4]. Among these

* Corresponding author. Xi'an University of Technology, Jinhua Road, Xi'an, 710048, PR China.

** Corresponding author. Xi'an University of Technology, 5 Jinhua Road, Xi'an, 710048, PR China.

E-mail addresses: zhonglisheng1984@163.com (L. Zhong), xuyunhua@xaut.edu.cn (Y. Xu).

coating materials, TiC is particularly noteworthy for its high elastic modulus, high hardness (2800 HV), high melting point ($3067\text{ }^{\circ}\text{C}$), low density (4.92 g/cm^3), good thermal stability, low friction coefficient and excellent wear resistance [5–7]. As one of the most promising advanced engineering structural materials, TiC is widely used for cutting tools, high-temperature ceramics, and wear-resistant components, including nozzles and bearings [8,9]. TiC-particulate-reinforced titanium-based surface composites have high potential for use in wear resistance applications because of their unique combination of properties, which include superior corrosion resistance, excellent wear resistance and a high strength-to-weight ratio [10–12].

The use of titanium or titanium alloys under severe wear conditions is highly restricted because of their poor tribological behaviors and low hardness [13,14]. Therefore, different surface

modification techniques have been used to deposit TiC coatings onto titanium or titanium alloy substrates, which include tungsten inert gas (TIG) welding [9,15,16], laser cladding (LC) [17,18], and chemical vapor deposition (CVD) [19,20]. A hard coating can be achieved through the TIG welding process using one of two approaches: (i) direct use of a ceramic or metallic powder to produce a hard coating or (ii) use of a cored wire associated with the welding process to fabricate a wear-resistant coating. Monfared et al. [9] used titanium-cored wires filled with micro-sized TiC particles and the TIG process to prepare TiC surface coatings on a pure titanium substrate. Their results indicated that the microstructure of the coating consisted of α -Ti, spherical and dendritic TiC particles. The volume fraction of TiC in the coating was 32.4%, the coating thickness was 2.1 mm, and the maximum hardness was 1073 HV_{0.2}, which is 7 times harder than the titanium substrate. LC technology employs a high-energy-density laser beam to heat a prefabricated coating material on the surface of a substrate; the coating material and the substrate surface then simultaneously melt and rapidly resolidify to form a surface coating. Savalani et al. [18] synthesized an in situ TiC/Ti coating on a pure titanium substrate by an LC-prepared and preplaced mixture of 20% carbon nanotubes and titanium powder. This coating was composed of α -Ti and coarse dendritic TiC particles, and the coating exhibited high hardness (1125 HV_{0.5}) and excellent wear resistance. In the CVD method, one or more gas-phase compounds or elements react with the substrate surface to form a thin film. Zhu et al. [20] synthesized an in situ TiC coating on a pure titanium substrate by the CVD method with a gas mixture of TiCl₄, CH₄ and H₂. The results showed that the thickness of the in situ deposited TiC coating was only approximately 6 μ m and that the hardness of the TiC layer was greater than 2000HV, which is approximately 15 times higher than that of pure titanium. Although these technologies can improve the abrasion resistance of coatings by increasing their surface hardness, numerous problems limit their range of applications. For TIG welding, additional carbide particles in the coating reduce the interfacial bonding strength and the volume fraction of carbide particles, which ranges from 11.2 to 32.4%, is also relatively low [9]. With LC, components easily segregate during the preparation of coatings, resulting in an uneven microstructure of the coating. CVD is limited to the preparation of thin coatings, and the lower toughness of these coatings limits their application, especially under heavy load and high-contact-stress working conditions [8,20]. In addition, some common disadvantages of these methods are the associated complex processes and high costs, which may also restrict their wider industrial applications. Therefore, preparation of a TiC coating with good wear resistance, high strength, and high toughness using a relatively low-cost and simple method has been the objective of extensive scientific and application-oriented research.

Here, we describe a low-cost, simple and very promising process for preparing TiC-Fe surface gradient coatings, namely, a two-step heat-treatment process. This process is based on the diffusion-controlled reaction of carbon and titanium to form a TiC-Fe coating during heat treatment. A pure titanium substrate provides a considerable amount of titanium, and a thin gray cast iron plate placed on the substrate surface provides an abundant carbon source for the in situ reaction. The two-step heat-treatment process has several clear advantages. First, when the heat-treatment

temperature and holding time are controlled, a surface gradient coating of a specific thickness can be prepared on a titanium matrix [21]. Moreover, the TiC/Ti interface exhibits a perfect metallurgical bond because of the in situ formation of TiC particles. In addition, a small amount of tough and strong bond-phase α -Fe distributed between the grains of the TiC can substantially improve the toughness and strength of the coating. In this study, TiC-Fe surface gradient coatings were successfully prepared on a titanium substrate via a simple two-step heat-treatment process. The microstructure, phase composition, mechanical properties, formation mechanism and toughening mechanism of the TiC-Fe surface gradient coating were systematically investigated.

2. Experimental procedures

2.1. Materials and preparation

Commercial pure titanium (CP-Ti) and gray cast iron (HT300) plate with dimensions of $10 \times 10 \times 10$ mm³ and $10 \times 10 \times 3$ mm³, respectively, were used as starting materials. The TiC-Fe surface gradient coating was prepared on the surface of pure titanium due to the reaction between titanium from CP-Ti and the graphite in the HT300 at 1150 °C for 5 min and then heat-treatment at 1000 °C for 10 h (1150 °C \times 5 min + 1000 °C \times 10 h). The phase compositions of CP-Ti and HT300 were α -Ti and α -Fe + lamellar graphite, respectively. The chemical compositions of the titanium and the HT300 were determined using a spectrum analyzer (EXF9600, Xifan, China) as shown in Table 1. The experimental procedure for the two-step heat-treatment process is shown in Fig. 1 and described as follows. First, the surface of the titanium substrate and the HT300 plate were sanded with SiC abrasive paper to remove the oxide coatings, which was then ultrasonically cleaned in acetone for 15 min. Second, the HT300 plate was placed on the surface of the titanium substrate, and then placed in a horizontal tube furnace (TF-1200, Kejing, China) at 1150 °C for 5 min. To avoid oxidation of the sample, pure argon gas was purged into the furnace tube throughout the heat-treatment process. The argon rate was controlled to 10 ml/min by adjusting an atmosphere valve. Then, the specimen was immediately covered with quartz sand to avoid crack generation and allowed to cool to room temperature naturally (first step of the heat treatment). The purpose of the first step of the heat treatment was to generate TiC nuclei at the interface between the HT300 and the titanium substrate to improve the interfacial wettability. Finally, the sample was subjected to heat treatment in the same manner at a lower temperature of 1000 °C for 10 h, the specimen was cooled to room temperature with the furnace (second step of the heat treatment). The purpose of the second step of the heat treatment was to facilitate the reaction between the titanium atoms and carbon atoms in the TiC-Fe coating. With this method, fine grains can be obtained because grain-boundary diffusion is maintained, and grain-boundary migration is effectively suppressed [22].

2.2. Characterization

To investigate the microstructures of the specimens' surface, the unreacted HT300 was ground off to expose the coating. The profile

Table 1
Chemical compositions of the HT300 plate and CP-Ti.

Element	C	Si	Mn	P	S	O	N	H	Cr	Fe	Ti
HT300	3.21	1.32	1.05	0.077	0.045	—	—	—	0.24	Balance	—
CP-Ti	0.01	—	—	—	—	0.008	0.01	0.005	—	0.02	Balance

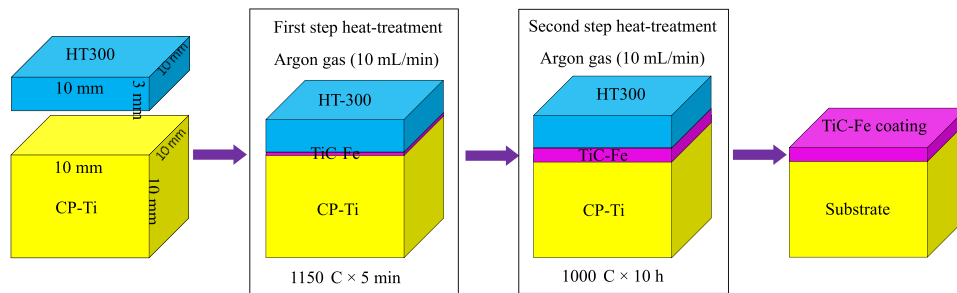


Fig. 1. Schematic diagrams of the two-step heat-treatment process.

and surface of the specimen were polished with a diamond paste and ultrasonically cleaned in acetone. The polished coating surface was then etched in a concentrated hydrochloric acid solution. The microstructure and the elemental distributions of the specimens were characterized by scanning electron microscopy (SEM, ZEISS, Germany) in conjunction with energy-dispersive X-ray spectrometry (EDS). The phase compositions and grain morphology of the TiC-Fe surface gradient coating were characterized by electron backscattered diffraction (EBSD, ZEISS, Germany). The cross section and surface of the specimen were analyzed by a Rigaku (Smartlap-9 kW) X-ray diffractometer (XRD, Japan) with Cu K α radiation at 45 kV and 200 mA in the 2θ range from 20° to 90° . The former did not grind off the remaining iron plate before the XRD test to demonstrate the formation of a titanium carbide phase during the in situ reaction of titanium and carbon, while the latter ground the remaining iron plate to identify the phase composition of the surface of the coating. In addition, Image-Pro Plus 6.0 software was used to calculate the volume fraction of the TiC phase [18]. The thickness of the TiC-Fe coating was measured by SEM.

2.3. Mechanical properties

A Nanoindenter G200 (Agilent Technologies, Oak Ridge, TN, USA) with a diamond Berkovich tip was used to measure the nanoindentation hardness (H) and elastic modulus (E) of the cross section of the TiC-Fe coating. The measurements were carried out at a constant strain rate of 0.02 s^{-1} to a maximum load of 450 mN. Loading and unloading lasted for 15 s each, and a holding of 10 s was implemented at the peak load value. For Palmqvist-type cracks, the following equation is used to estimate the fracture toughness (K_C) [23]:

$$K_C = k \left(\frac{a}{l} \right)^{1/2} \left(\frac{E}{H} \right)^{2/3} \frac{P}{c^{3/2}} \quad (1)$$

where k is a constant with a value of 0.016 for a Berkovich tip, a is the half-diagonal of the indentation imprint, l is the crack length, E is the elastic modulus, H is the nanoindentation hardness, P is the indentation load, and c is the sum of a and l . Here, the lengths of the half-diagonal of the indentation imprint and the crack were measured using Smile View software [24].

2.4. Single-scratch testing

Scratch tests were performed on the polished coating surface at room temperature using a WS-2005 automatic scratch tester (WS-2005, China) with a spherical diamond indenter. The load was linearly increased from 0 N to 100 N with a loading rate of 100 N/min and a constant scratching speed of 0.05 mm/s. The scratch tests were carried out in different regions on the specimen under the same conditions with a scratch length of 3 mm.

3. Results and discussion

3.1. Characterization and microstructure of the TiC-Fe surface gradient coating

The phase composition of the in situ-formed TiC surface gradient coating on a pure titanium substrate was characterized by XRD, as shown in Fig. 2. Fig. 2(a) shows the XRD pattern of the cross section of the specimen. The pattern presents characteristic peaks of the TiC (cubic system, space group $Fm\bar{3}m$ (225), International Center for Diffraction Data (ICDD) card No. 32-1383), Ti (hexagonal

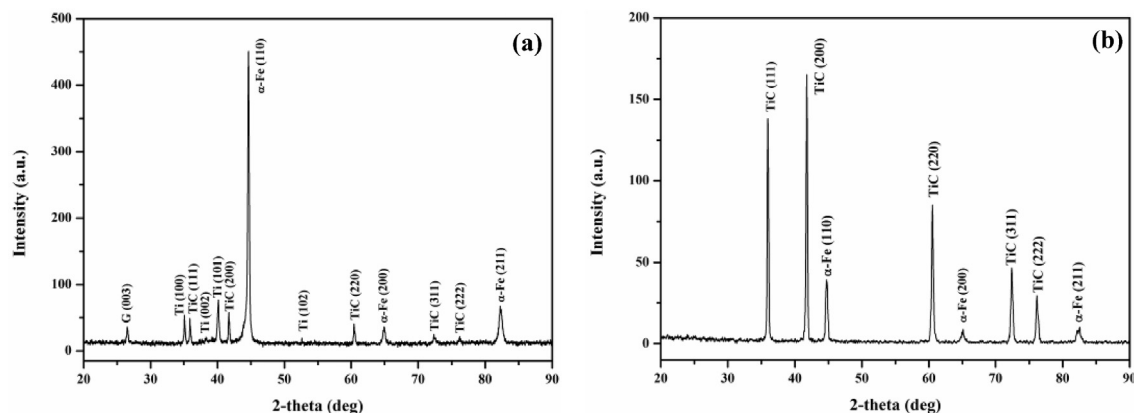


Fig. 2. XRD pattern of (a) the cross section and (b) the surface of the in situ TiC-Fe surface gradient coating on a titanium substrate at $1150^\circ\text{C} \times 5 \text{ min} + 1000^\circ\text{C} \times 10 \text{ h}$.

system, space group $P6_3/mmc$ (194), ICDD card No. 44-1294), α -Fe (cubic system, space group $Im-3m$ (229), ICDD card No. 06-0696) and graphite (G) phases (hexagonal system, space group $P6_3mc$ (186), ICDD card No. 26-1076). XRD peaks appeared at 2θ had values of 35.906, 41.710, 60.448, 72.369 and 76.139 corresponding to the (111), (200), (220), (311) and (222) peaks, indicating the formation of TiC phase. Since the remaining iron plate was not ground off before the XRD analysis, a strong α -Fe diffraction peak was exhibited in Fig. 2(a). Fig. 2(b) presents the XRD pattern of the surface of the TiC-Fe coating; the pattern indicates that α -Fe and TiC particles are the main phases. The remaining iron plate was ground off before the surface of the coating was characterized by XRD. The α -Fe diffraction peak originates from the contribution of the α -Fe phase in the coating. Since the content of the α -Fe phase in the coating is small, the diffraction intensity is weak relative to the α -Fe diffraction peak in Fig. 2(a).

Fig. 3 presents the typical cross sectional microstructure for the TiC-Fe surface gradient coating on a pure titanium substrate at $1150^\circ\text{C} \times 5\text{ min} + 1000^\circ\text{C} \times 10\text{ h}$. The TiC-Fe coating is sandwiched between the unreacted HT300 and the titanium substrate (Fig. 3(a)). The coating is dense and possesses a mean thickness of approximately $30.4 \pm 1.1\ \mu\text{m}$. Moreover, the interface between the coating and the substrate exhibited neither cracks nor pores, demonstrating perfect metallurgical bonding. To further understand the chemical compositions of the coating, EDS characterization was performed at different regions of the cross section of the TiC-Fe surface gradient coating, as indicated in Fig. 3(a). The atomic ratios of titanium, carbon and iron corresponding to EDS regions 1, 2 and 3 are 35.09:44.61:20.30, 47.54:47.70:4.76 and 50.77:48.38:0.85, respectively. In addition, the elemental mapping micrographs for the cross-section view of the TiC-Fe surface gradient coating on a titanium substrate are shown in Fig. 4. According to the distribution of the elements and XRD analyses (Fig. 2), the white phase represents the α -Fe phase, and the black phase represents the TiC phase in the TiC-Fe coating. Moreover, as the thickness of the coating increases, the iron content clearly decreases, and the titanium and carbon contents clearly increase, indicating that the composition of the TiC-Fe coating represents a

gradient distribution. Thus, along the vertical direction from the HT300 to the titanium substrate, the TiC-Fe surface gradient coating can be divided into three zones according to the volume fraction of the TiC particulates and α -Fe (Fig. 3). The thickness and TiC volume fraction of the different zones of the cross-section of the TiC-Fe coating are shown in Table 2. Therefore, based on the aforementioned analysis of the microstructure features, the TiC-Fe coating with a dense and gradient structure was successfully prepared by the two-step heat-treatment process.

Fig. 5 shows the microstructure and EDS analysis results for the surface of the TiC-Fe coating on a titanium substrate treated at $1150^\circ\text{C} \times 5\text{ min} + 1000^\circ\text{C} \times 10\text{ h}$. The surface microstructure of the TiC-Fe coating is presented in Fig. 5(a) after the remainder of the HT300 had been ground off and etched with concentrated hydrochloric acid solution. This microstructure is consistent with the XRD results (Fig. 2(b)), indicating that the α -Fe phase is distributed along the grain boundaries of the TiC particles. The magnified image of region b is shown in Fig. 5(b). The grain size of an ovaloid TiC particle is approximately $1\ \mu\text{m}$, and some of the small TiC particles are intertwined and connected to each other rather than dispersed as single granules. The quantitative elemental analysis by EDS indicates that the ovaloid particles were composed only of titanium and carbon at an atomic ratio of approximately 1:1 (Fig. 5(c)), which were confirmed via the XRD analysis to be in the TiC phase (Fig. 2(b)).

To gain a better understanding of the phase composition and grain morphology of the TiC-Fe surface gradient coating, its cross section was further characterized by EBSD. Fig. 6 presents the EBSD images of a cross section of the TiC-Fe surface gradient coating in the normal direction (ND). Fig. 6(a) shows the band contrast image of a cross section of the TiC-Fe surface gradient coating from the EBSD analysis. Carbide particles with different sizes and shapes are present in the different zones of the coating. Therefore, according to the size and shape of the carbide particles, the TiC-Fe surface gradient coating can be artificially divided into three zones: a columnar TiC zone (I zone), a large particle TiC zone (II zone) and a large bulk TiC zone (III zone), consistent with the three zones depicted in Fig. 3(a). The phase distribution map for the coating

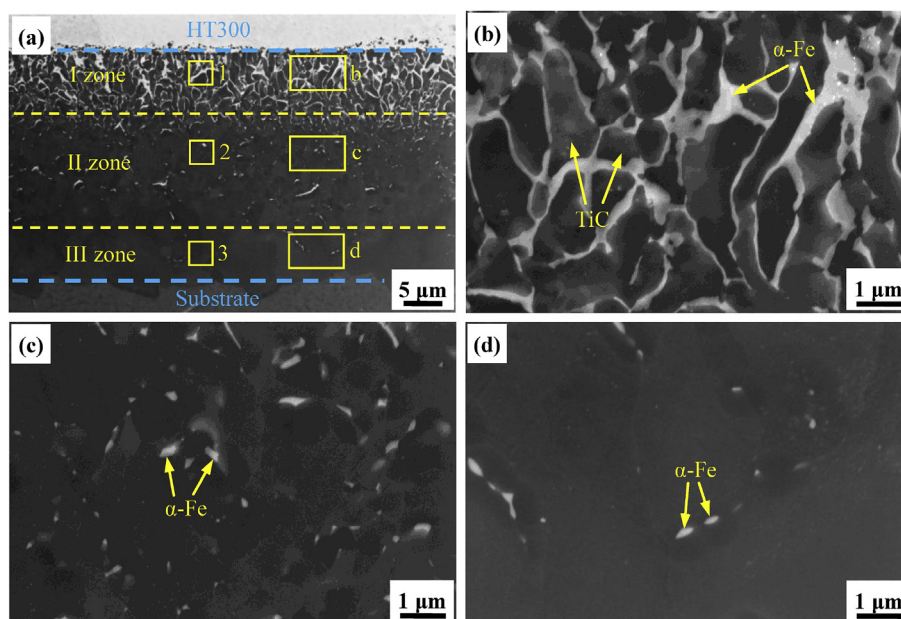


Fig. 3. Cross sectional SEM images of (a) microstructural overview, (b) I zone, (c) II zone, (d) III zone. As indicated in (a), the in situ TiC-Fe surface gradient coating formed on a titanium substrate at $1150^\circ\text{C} \times 5\text{ min} + 1000^\circ\text{C} \times 10\text{ h}$.

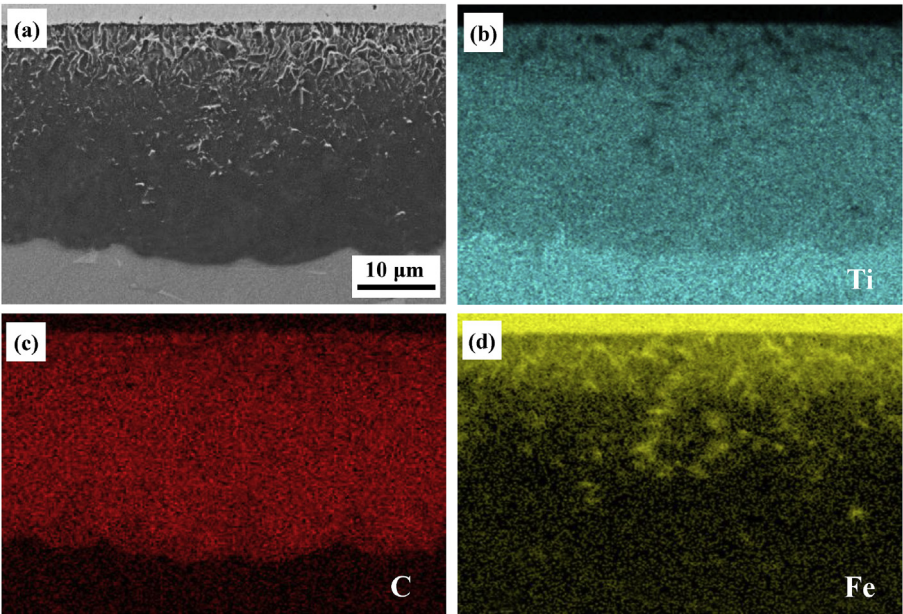


Fig. 4. Microstructure and elemental mapping micrographs for the cross sectional view of the TiC-Fe surface gradient coating on a titanium substrate: (a) SEM image, and (b–e) mapping micrographs for Ti, C and Fe.

Table 2
Thickness and TiC volume fraction of different zones of the cross section of the TiC-Fe coating.

Zones	Volume fraction of TiC (%)	Thickness (μm)
I zone	76.4 ± 2.1	9.4 ± 1.4
II zone	96.2 ± 1.3	11.9 ± 1.6
III zone	99.3 ± 0.5	9.1 ± 1.3

cross section is presented in Fig. 6(b). This map shows the presence of two crystallized phases—a harder TiC and a ductile α -Fe—within

the coating, which is consistent with the XRD results (Fig. 2(a)). These results indicate that the graphite phase in the HT300 reacted with the titanium to form a TiC-Fe surface gradient coating on the titanium substrate. High-magnification EBSD images of the different zones of the cross section of the TiC-Fe coating are shown in Fig. 7. As shown in Fig. 7(a), the TiC grain morphology is a columnar structure with a length of 2–5 μm and a diameter of approximately 1 μm. Fig. 7(d) shows that the grain morphology is a large particle structure and that the mean grain size is approximately 2.82 μm. Large bulk TiC ceramic particles are observed at the

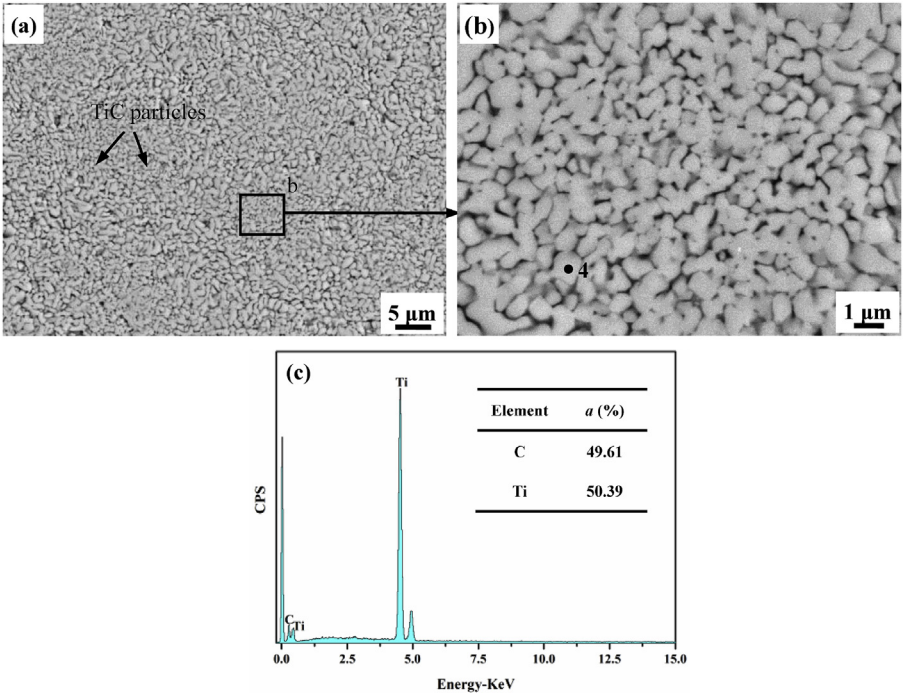


Fig. 5. (a) and (b) the microstructure and (c) EDS results for a TiC particle on the surface of the TiC-Fe coating on a titanium substrate treated at 1150 °C × 5 min + 1000 °C × 10 h.

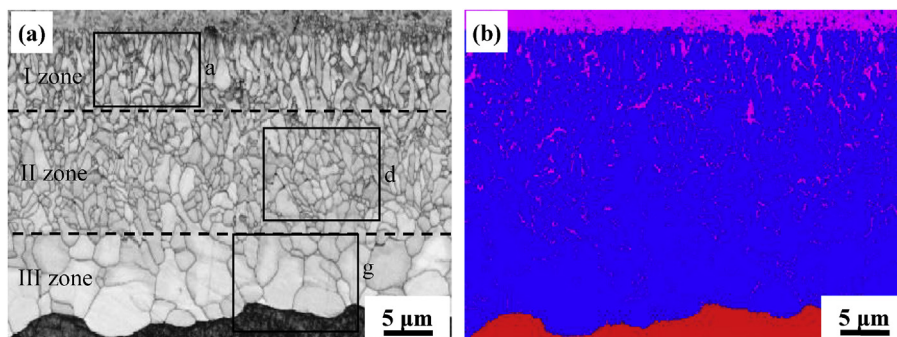


Fig. 6. EBSD images of a cross section of the TiC-Fe surface gradient coating: (a) band contrast map and (b) phase map (fuchsia: α -Fe, blue: TiC, red: α -Ti). (For interpretation of the references to color in this figure legend, the reader is referred to the Web version of this article.)

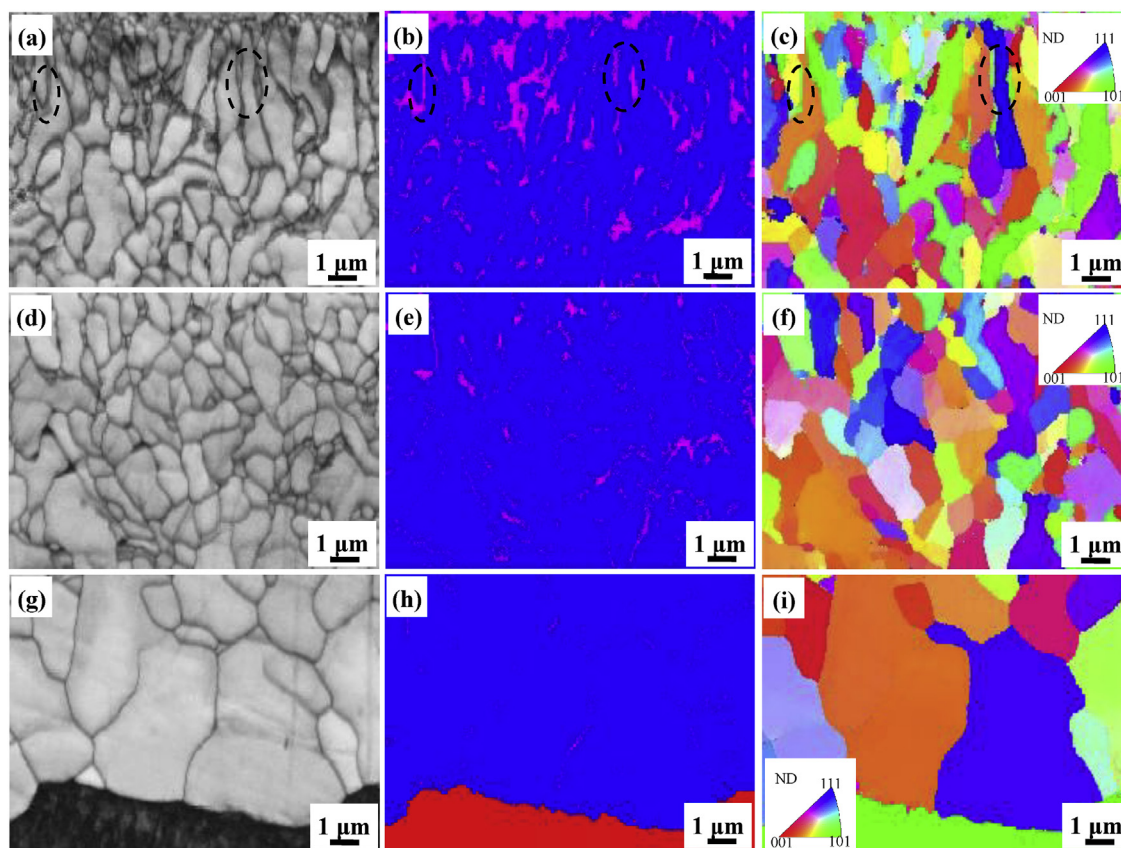


Fig. 7. High-magnification EBSD images of different zones of a cross section of the TiC-Fe surface gradient coating: (a), (b) and (c) I zone; (d), (e) and (f) II zone; (g), (h) and (i) III zone, as indicated in Fig. 6(a).

coating/substrate interface, and the average grain size is approximately 5.56 μm , as shown in Fig. 7(g). The interface between the TiC coating and the substrate exhibits a high-quality metallurgical bond. Fig. 7(b,e,h) indicate that the α -Fe phase is distributed along the grain boundaries of the TiC particles and that the volume fraction of the α -Fe phase decreases as the thickness of the coating increases. Fig. 7(c,f,i) show the detailed EBSD maps of the grains colored based on their orientation. The orientations of these grains can be indexed to the inserted inverse pole figures, as shown by the different colors in the map. The columnar TiC grains have a prominent growth orientation perpendicular to the HT300/coating interface (Fig. (c)), which may be related to the direction of carbon diffusion. Fig. 7(f,i) indicate that the large particles TiC and the large

bulk TiC particles have no preferred orientation distribution. It is particularly noteworthy that all α -Fe phases are shown in one color (green), indicating that the α -Fe phase grows mainly along the (101) direction. This may be related to the infiltration of iron. Therefore, the grain size and the volume fraction of the TiC phase increase and the content of the α -Fe phase decreases with increasing depth from the interface of the HT300/TiC coating to the substrate. Moreover, the TiC particles have different morphologies at different locations along the cross section of the TiC-Fe surface gradient coating and exhibit morphological characteristics such as columnar, large particle and large bulk.

Fig. 8 shows the EBSD images of the surface of the TiC-Fe coating in the ND. Fig. 8(a) shows a band contrast map of the surface of the

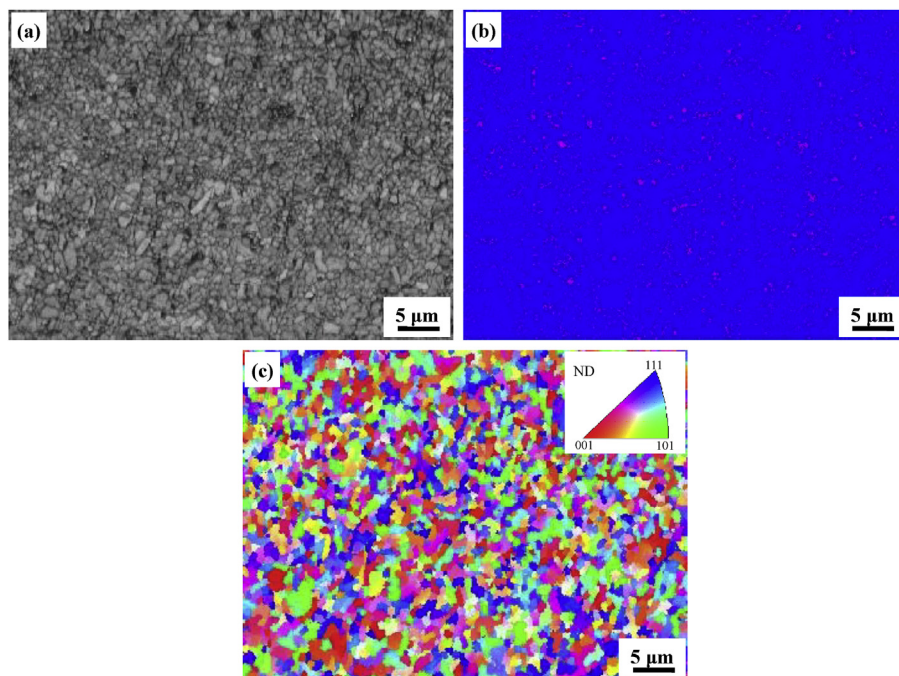


Fig. 8. EBSD measurement for the surface of the TiC-Fe surface gradient coating: (a) band contrast map; (b) phase map (fuchsia: α -Fe, blue: TiC); and (c) orientation image map (OIM). (For interpretation of the references to color in this figure legend, the reader is referred to the Web version of this article.)

coating. The ovaloid TiC grains are approximately 1 μm in diameter. Fig. 8(b) presents the phase distribution map of the surface of the TiC-Fe coating. This map verifies that the coating consisted of TiC and α -Fe, with no other phases, and that the volume fraction of the TiC particles was approximately 77%. These results are supported by the XRD results (Fig. 2(b)) and the SEM analysis results (Fig. 5(a)). The orientation map in Fig. 8(c) indicates no preferred orientation distribution in the TiC grains. On the basis of the aforementioned analysis, the surface of the TiC-Fe coating matches the I zone of the cross section of the TiC-Fe surface gradient coating.

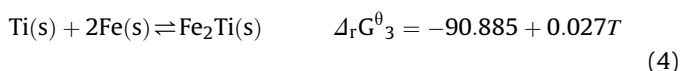
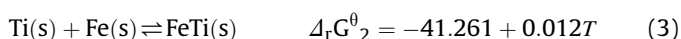
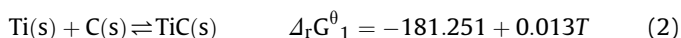
Therefore, based on the aforementioned detailed analysis of the microstructural characteristics, the microstructure of the TiC-Fe coating prepared by the two-step heat-treatment process has the following unique advantages. (i). The coating contains a high volume fraction of the hard-phase TiC (>90%). (ii). The coating has a gradient distribution structure. As the thickness of the coating increases, the size of the titanium carbide particles increases, and the volume fraction of the α -Fe phase decreases. (iii). The coating contains a small amount of tough α -Fe phase, which gives the surface of the coating the microstructural characteristics of high hard-phase TiC + high tough-phase α -Fe, thus improving the coating toughness. However, due to the small amount of α -Fe phase present in the coating, galvanic corrosion may occur due to the potential difference between the α -Fe phase and TiC.

3.2. Formation mechanism of the TiC-Fe surface gradient coating

The TiC-Fe surface gradient coating was produced on a pure titanium substrate via the two-step heat-treatment process at $1150^\circ\text{C} \times 5 \text{ min} + 1000^\circ\text{C} \times 10 \text{ h}$. Based on the Fe-C, Fe-Ti, and Ti-C phase diagrams [6,25] in the heat-treatment temperature range of 1000 – 1150°C , a Ti-C-Fe ternary system can be obtained at the interface between the HT300 and the titanium substrate [26–28]. Therefore, to gain a better understanding of the formation process and the mechanism of the TiC-Fe surface gradient coating, the coating formation was analyzed on the basis of standard Gibbs free

energy, the nucleation-growth theory and the solid-phase diffusion theory.

In the Ti-C-Fe system, the possible reactions and the corresponding Gibbs free energy changes as functions of temperature are described as follows [25,29,30]:



The Gibbs free energies calculated for the TiC, FeTi, Fe_2Ti , and Fe_3C phases according to the reactions in equations (2)–(5) are plotted in Fig. 9 as functions of temperature. At the heat-treatment temperatures (1000°C and 1150°C), the Gibbs free energies of TiC, Fe_2Ti , FeTi, and Fe_3C are negative, implying that all these reactions can occur. A smaller Gibbs free energy value corresponds to a larger driving force of the reaction and a more stable product. The Gibbs free energy of TiC, $\Delta_r G_1^\theta$, is lower than that of Fe_2Ti , FeTi and Fe_3C . Therefore, the TiC phase is the most thermodynamically favored phase and is a more stable product than the other three phases in the reaction system.

Titanium is well known to be a strong carbide-forming element and has a larger negative heat of formation with carbon at 1150°C (-166.3 kJ/mol), indicating that titanium atoms and carbon atoms experience a substantial driving force to form TiC [19]. Therefore, during the first step heat-treatment process (1150°C), [TiC] forms in the melt pool by the in situ reaction between [Ti] and [C], where the Ti atoms desolvate from the titanium substrate; in addition, the C atoms desolvate from the flake graphite in the HT300. When the concentration of [TiC] reaches saturation, TiC nuclei

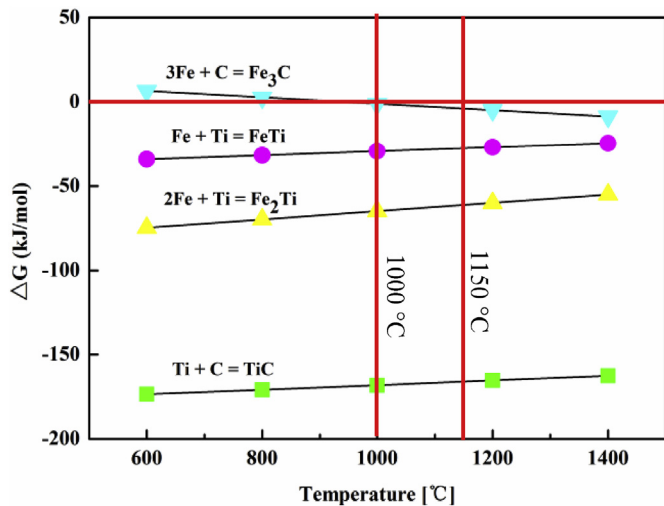


Fig. 9. Curves of the Gibbs free energy of the possible products as a function of temperature.

precipitate and grow. As the reaction progresses, a thin TiC coating is formed between the titanium substrate and the HT300, as shown in Fig. 10(a). Moreover, some high-energy iron passes through the dense TiC coating into the grain boundary of the TiC particles. During the second step heat-treatment process (1000 °C), the carbon atoms supplied by the graphite via diffusion react with titanium atoms supplied by the titanium substrate to form TiC. The carbon atom radius (0.091 nm) is smaller than that of the titanium atom (0.200 nm), leading to different diffusion mechanisms. Carbon atoms move via interstitial diffusion and titanium atoms move via void diffusion in the TiC-Fe coating during the heat treatment, which results in the diffusion velocity of the carbon atoms in the TiC-Fe coating being significantly faster than that of the titanium

atoms during the heat treatment [31]. Thus, the growth of the coating is controlled by the diffusion of carbon into the carbide coating. Moreover, Miriyev et al. [27] have confirmed via inert labeling experiments that the growth kinetics of the TiC coating are controlled by the diffusion of carbon from the carbon steel to the titanium alloy through the TiC phase. Therefore, after a thin TiC-Fe coating is formed between the titanium substrate and the HT300, the interface of the TiC-Fe coating/Ti substrate moves perpendicularly toward the titanium substrate, as shown in Fig. 10(a) [32]. Due to the in situ extension of the TiC-Fe coating, the TiC-Fe coating/substrate interface can achieve a metallurgical combination. In Fig. 7, the microstructure characteristics of the coating gradually variation with increasing coating depth, including the size and morphology of the TiC particles in the coating. Both the carbon atom concentration and the iron content play important roles in determining the size and morphology of the TiC grains. An equation for the distribution of carbon in the TiC-Fe surface gradient coating is presented as [27].

$$C = C_s - (C_s - C_0) \operatorname{erf} \left[\frac{x}{2\sqrt{Dt}} \right] \quad (6)$$

where C is the carbon concentration in the TiC-Fe surface gradient coating, C_s is the carbon concentration in the HT300, C_0 is the carbon concentration in the titanium substrate, x is the coating thickness, D is the diffusion coefficient of carbon atoms in the TiC-Fe coating, and t is the treatment time. Fig. 10(b) shows the variation in the carbon concentration with TiC-Fe coating thickness. The diffusion rate of carbon atoms decreases with increasing coating thickness. At the I zone, because of the gradient of the carbon concentration and the rapid heating and cooling during the first-step heat treatment, TiC grains may grow directionally, leading to the formation of columnar TiC grains. The carbon atoms diffuse through the grain boundaries of the TiC particles in the I zone to enter the II zone and react with the titanium substrate to form TiC. With the continuous diffusion of carbon atoms, the carbon atoms can react sufficiently with titanium. However, in the II zone, the carbon concentration is much lower than that in the I zone; therefore the newly formed small TiC particles gradually grow into large particle. The driving force for the diffusion of carbon atoms into the III zone is lower than that for the diffusion of carbon atoms into the I zone and II zone. Accordingly, the nucleation density is gradually reduced, resulting in a dramatic increase in TiC grain size. Therefore, the TiC grain size is largest in the III zone. In addition, the increased iron content also decreases the reaction temperature and the dwell time of the in situ reaction at high temperatures, resulting in a decrease in TiC particle size [33]. Moreover, the presence of iron usually changes the growth rate of TiC along the $\langle 100 \rangle$ and $\langle 111 \rangle$ directions, which leads the TiC to form other shapes [34]. Therefore, on the basis of this analysis, the actual morphology and size of the TiC crystals are determined by the interaction of these two factors and are closely related to factors that affect growth kinetics, such as interface properties and mass transport processes [35].

To elucidate the formation mechanisms of the TiC-Fe surface gradient coating, the phase transformation process was investigated. The phase transformation diagram of titanium to TiC is presented in Fig. 11. When the temperature is greater than 882.5 °C, the titanium substrate is transformed from the hexagonal close-packed (hcp) α -Ti to body-centered cubic (bcc) β -Ti. Fig. 11(a) shows a β -Ti lattice with a lattice constant of $a = b = c = 0.3306$. The interstitial carbon atoms enter the vacancies of the β -Ti lattice by diffusion. To clearly show the position of the carbon atoms in the β -Ti lattice, octahedral vacancies in the β -Ti superlattice are illustrated in Fig. 11(b). The carbon atoms clearly occupy positions on the center of the axis or in the plane of the titanium lattice.

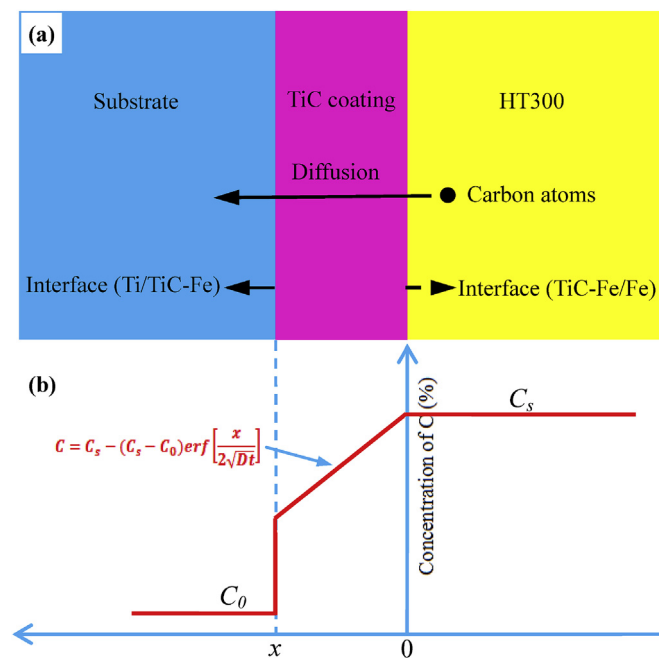


Fig. 10. Schematic diagrams of (a) the growth of the TiC-Fe coating at the TiC-coating/Ti interface by the diffusion of carbon and at the TiC-Fe coating/Fe interface by the diffusion of titanium and (b) the variation of the carbon concentration with TiC-Fe coating thickness.

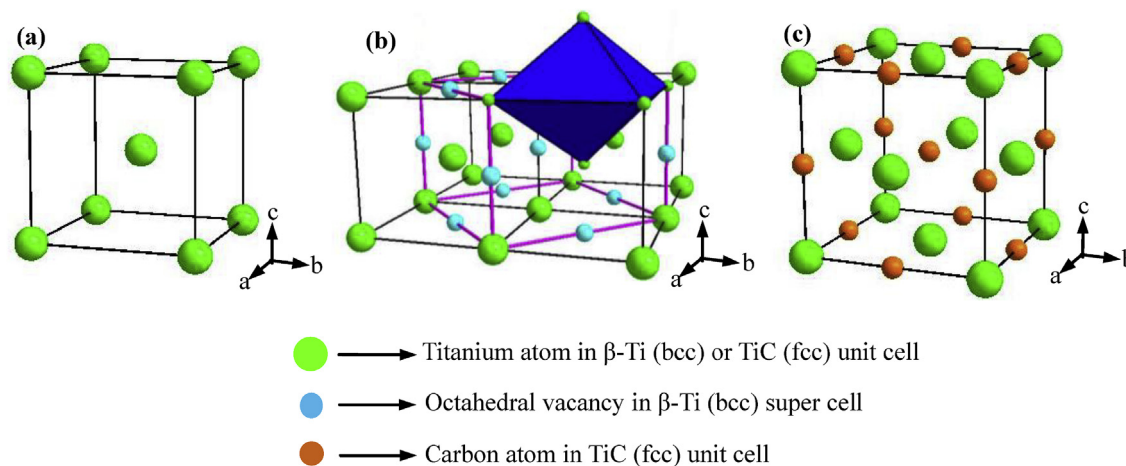


Fig. 11. Schematic diagrams showing the crystal structure transformation: (a) unit cell of bcc β -Ti; (b) supercells of bcc β -Ti with octahedral vacancies; and (c) the unit cell of fcc TiC.

Moreover, the positions of the carbon atoms in the fcc TiC lattice ($a = b = c = 0.4328$) are coincident with the octahedral voids in the β -Ti lattice (Fig. 11(c)). The radius of a tetrahedral vacancy is larger than that of an octahedral vacancy in the bcc β -Ti lattice, with carbon atoms preferentially occupying an octahedral vacancy due to effective strain relief [36].

3.3. Mechanical properties and toughening mechanism of the TiC-Fe surface gradient coating

The nanoindentation hardness and elastic modulus values of the cross section of the coating along the thickness direction were measured; the results are shown in Fig. 12. Based on the above description of the microstructural characteristics (Figs. 3(a) and 6(a)), the nanoindentation hardness and elastic modulus profiles are clearly divided into three zones. At a depth of 9 μm (I zone), the average values of the nanoindentation hardness and elastic modulus are 21.8 GPa and 389.1 GPa, respectively. At a depth between 9 μm and 21 μm (II zone), the average values of the nanoindentation hardness and elastic modulus are 28.1 GPa and 430.8 GPa, respectively. Furthermore, at a depth between 21 μm

and 30 μm (III zone), the nanoindentation hardness and elastic modulus reach their highest values of approximately 31.7 GPa and 464.3 GPa, respectively. This gradual increase in mechanical properties is attributed to the formation of the gradient microstructure of the TiC volume fraction and the grain size in the coating. Clearly, the in situ TiC-Fe surface gradient coating shows a remarkable improvement in hardness (6–11 times) and elastic modulus (2–4 times) compared with those of the titanium substrate (2.8 GPa and 137.3 GPa, respectively). Fig. 13 shows the details of the nanoindentation imprints at different zones of the cross section of the TiC-Fe surface gradient coating under an applied load of 450 mN. The cracks appear to emanate from the corners of the indentation, without chipping. Using the nanoindentation hardness, elastic modulus, and crack length obtained from the nanoindentation experiments, the fracture toughness of the TiC-Fe surface gradient coating was calculated by equation (1). The fracture toughness values of the I zone, II zone and III zone are $(3.5 \pm 0.15) \text{ MPa} \cdot \text{m}^{1/2}$, $(1.9 \pm 0.14) \text{ MPa} \cdot \text{m}^{1/2}$ and $(3.1 \pm 0.21) \text{ MPa} \cdot \text{m}^{1/2}$, respectively. These results indicate that the fracture toughness varies considerably depending on the composition and the microstructure.

To better understand the toughening mechanism, the surface morphologies of the cracks were investigated. Fig. 13(d) and (e) show the details of the indentation crack morphology of the I zone (Fig. 13(a)). The crack propagation is characterized by a zigzag path (Fig. 13(d)), which indicates that crack deflection occurred during its propagation. In the process of crack propagation, because of interface mismatches and their different mechanical features, a high interfacial strain field can form between the TiC grains and the α -Fe phase [37]. Therefore, when the crack tip reaches the strain field, the stress concentration accumulates in the interface of the TiC grains and the α -Fe phase, resulting in a crack that continues to expand along the low fracture energy interfaces (grain boundaries), which causes crack propagation along the grain boundary. The total length of the crack would increase once the crack is deflected, and this will enhance the energy consumption and decrease the driving force of crack propagation [37,38]. Thus, crack deflection plays a role in improving the toughness of the coating. Additionally, crack bridging is also observed in radial crack propagation, and the bridging phases between the crack surfaces contain ductile α -Fe and brittle TiC; the former contributes to toughness through plastic dissipation as a ligament bridge. When these ligaments eventually fail in the crack wake, energy is dissipated as acoustic waves and causes toughening. The latter is understood by recognizing that large local residual stresses suppress local crack propagation [38].

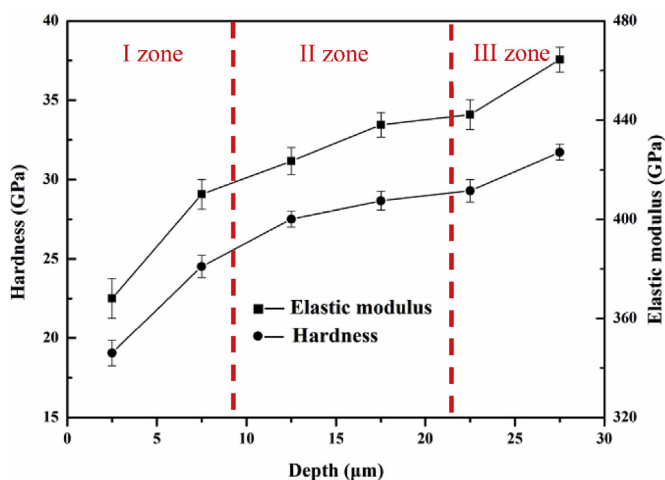


Fig. 12. The nanoindentation hardness and elastic modulus distributions of the TiC-Fe surface gradient coating along the thickness direction.

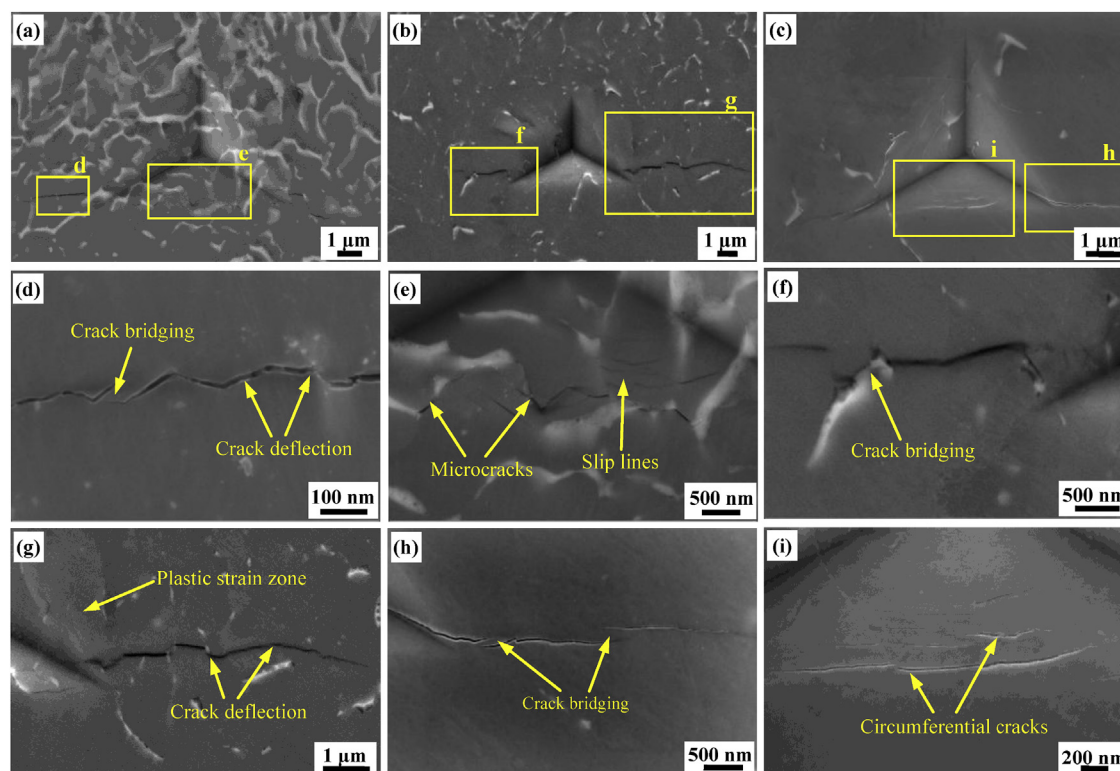


Fig. 13. Details of nanoindentation imprints at different zones of the cross section of the TiC-Fe surface gradient coating at an applied load of 450 mN.

Moreover, microcracks and slip lines are observed inside the residual imprint and at the indentation edges (Fig. 13(e)), respectively. Fig. 13(f) and (g) show details of the indentation crack morphology of the II zone (Fig. 13(b)). Crack bridging (Fig. 13(f)) and crack deflection (Fig. 13(g)) are also observed in this zone. Additionally, a plastic strain zone is observed at the indentation edges (Fig. 13(g)). The details of the indentation crack morphology of the III zone (Fig. 13(c)) are depicted in Fig. 13(h) and (i). Crack bridging is observed in the radial crack propagation (Fig. 13(h)). In addition to the radial cracks, larger circumferential cracks are found inside the residual imprint and at the indentation edges (Fig. 13(i)). In the case of large bulk TiC particles, the crack tip will generate a large strain stress field and come across the TiC grain at a certain angle in the direction of crack propagation, forming a transgranular crack. Moreover, residual stress-induced bridging occurs because circumferential compression causes the crack to circumvent local, highly stressed regions [38]. In addition, in the process of loading, the larger tensile stress component induces the occurrence of the largest crack. The formation of a circumferential crack consumes a large amount of energy, reducing the stress at the crack tip and increasing crack propagation resistance, thereby toughening the coating. This toughening likely accounts for the greater fracture toughness in large bulk TiC zones than in large particle TiC zones. Much remains to be studied and investigated on this issue. Nevertheless, on the basis of the aforementioned analysis, crack bridging, crack deflection and microcracking can increase the total length of a crack, which can cause an enlargement of the fracture area [38,39]. This enlarged fracture area will enhance energy consumption and diminish the driving force of crack propagation [40]. Therefore, crack bridging, crack deflection and microcracking can lead to resistance to crack propagation and, therefore, substantially improve the toughness of the coating.

3.4. Single scratch test results

To further evaluate the adhesion strength between the coating and the substrate, scratch tests were performed on the surface of the TiC-Fe coating. Fig. 14 shows the macroscopic morphology of the scratch track on the surface of the TiC-Fe composite coating after the scratch test. Fig. 14(a) shows the global view of the scratched coating surface. The width of the scratch track increases linearly as the applied load increases (0–100 N). Fig. 14(b and c) display the highlighted morphology of the scratch groove, as indicated in Fig. 14(a). Lateral cracks appear at the bottom of the scratch groove because during scratching, compressive stresses are induced in the coating ahead of the moving indenter, whereas tensile stresses are induced at the trailing edge of stylus [41]. This pull causes local lateral cracks at the bottom of the scratch groove. Fig. 14(d and e) show the lateral crack morphology at the bottom of the scratch groove. Crack deflection is observed in lateral crack propagation. In addition, at 100 N, only the near-surface chips are peeled off (Fig. 14(c)), and more TiC particles are pulled out on the fracture surface (Fig. 14(f)), indicating that the adhesion strength of the coating/substrate is higher than its inner cohesive strength. This difference is mainly due to the distribution of a small amount of high-toughness α -Fe phase in the coating and the gradient change of the microstructure. Therefore, the adhesion strength of the TiC-Fe coating is significantly improved over that of the pure TiC coating [42].

4. Conclusions

In this research, a novel TiC-Fe surface gradient coating was successfully prepared on a pure titanium substrate by a simple two-step heat-treatment process ($1150\text{ }^{\circ}\text{C} \times 5\text{ min} + 1000\text{ }^{\circ}\text{C} \times 10\text{ h}$). The microstructures and mechanical properties of the TiC-Fe

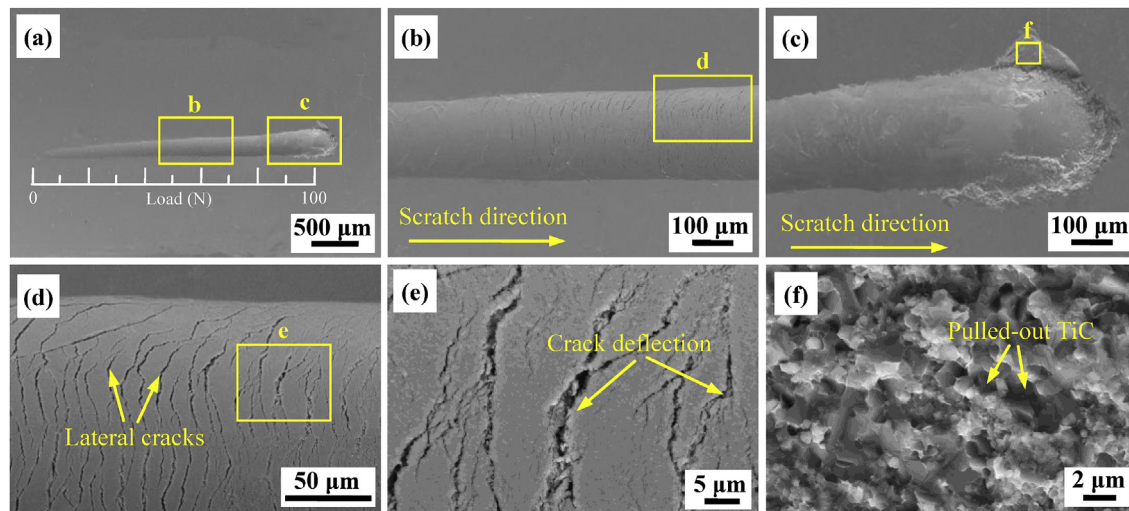


Fig. 14. SEM image of the corresponding residual scratch path morphology of the TiC-Fe coating under ramp loading conditions to a maximum load of 100 N: (a) global view of the scratched coating surface; (b, c) corresponding magnified views of the scratch path as indicated in (a); (d) highlighted morphologies of the scratch groove as illustrated in (b); (e) corresponding magnified views of the crack morphology as indicated in (d); and (f) fracture surface under a peeled chip at 100 N as indicated in (c).

surface gradient coating were investigated. The results indicate the following:

- (1) The TiC-Fe surface gradient coating consisted mainly of three zones: a columnar TiC zone (I zone), a large particle TiC zone (II zone) and a large bulk TiC zone (III zone). The formation process and mechanism for the TiC-Fe surface gradient coating consisted of nucleation growth of TiC grains as well as diffusion and in situ reactions between titanium and carbon.
- (2) The maximum nanoindentation hardness and elastic modulus of the TiC-Fe surface gradient coating were 31.7 GPa and 464.3 GPa, respectively. However, the fracture toughness value was $3.1 \text{ MPa m}^{1/2}$. Meanwhile, the coating exhibited excellent coating/substrate adhesion strength.
- (3) Due to the presence of high volume fraction (>90%) and high hardness TiC in the TiC-Fe surface gradient coating, the coating exhibited high hardness and elastic modulus. At the iron-rich location of the TiC-Fe gradient coating, the toughening mechanism was a mixture of crack deflection, grain bridging and intergranular fracture. However, at the iron-poor location of the TiC-Fe gradient coating, the toughening mechanism was a mixture of crack bridging, circumferential cracking and transgranular fracture. Thus, the presence of high tough-phase α -Fe in the coating and the gradient variation of the microstructure were the main reasons for the TiC-Fe gradient coating exhibiting high toughness and excellent coating/substrate adhesion strength.

Acknowledgments

The project was supported by the National Natural Science Foundation of China (Grant No. 51501148 and 51704232), the Key-point Research and Invention Program of Shaanxi Province (Grant No. 2017ZDXM-GY-032) and the Project of the Shaanxi Key Laboratory of Nano Materials and Technology (Grant No. 15JS054).

References

- [1] J. Li, Y. Zhang, Y. Zhao, Mechanical properties of TiN ceramic coating on a heat treated Ti-13Zr-13Nb alloy, *J. Alloys Compd.* 724 (2017) 34–44.
- [2] D. Tijo, M. Masanta, Mechanical performance of in-situ TiC-TiB 2 composite coating deposited on Ti-6Al-4V alloy by powder suspension electro-discharge coating process, *Surf. Coating. Technol.* 328 (2017) 192–203.
- [3] X.S. Fan, Z.G. Yang, Z.X. Xia, C. Zhang, H.Q. Che, The microstructure evolution of VC coatings on AISI H13 and 9Cr18 steel by thermo-reactive deposition process, *J. Alloys Compd.* 505 (2010) L15–L18.
- [4] Y. Long, A. Javed, J. Chen, Z. Chen, X. Xiong, The effect of deposition temperature on the microstructure and mechanical properties of TaC coatings, *Mater. Lett.* 121 (2014) 202–205.
- [5] X. Wang, H. Ding, F. Qi, Q. Liu, X. Fan, Y. Shi, Mechanism of in situ synthesis of TiC in Cu melts and its microstructures, *J. Alloys Compd.* 695 (2017) 3410–3418.
- [6] H.L. Yu, W. Zhang, H.M. Wang, X.C. Ji, Z.Y. Song, X.Y. Li, B.S. Xu, In-situ synthesis of TiC/Ti composite coating by high frequency induction cladding, *J. Alloys Compd.* 701 (2017) 244–255.
- [7] W. Lu, D. Zhang, X. Zhang, R. Wu, T. Sakata, H. Mori, Microstructural characterization of TiC in in situ synthesized titanium matrix composites prepared by common casting technique, *J. Alloys Compd.* 327 (2001) 248–252.
- [8] B. Liu, S. Huang, J.V. Van Humbeeck, J. Vleugels, Influence of Mo addition on the microstructure and mechanical properties of TiC-NiTi cermets, *J. Alloys Compd.* 712 (2017) 579–587.
- [9] A. Sivkov, I. Shanenkov, A. Pak, D. Gerasimov, Y. Shanenkova, Deposition of a TiC/Ti coating with a strong substrate adhesion using a high-speed plasma jet, *Surf. Coating. Technol.* 291 (2016) 1–6.
- [10] Y. Qin, L. Geng, D. Ni, Dry sliding wear behavior of extruded titanium matrix composite reinforced by in situ TiB whisker and TiC particle, *J. Mater. Sci.* 46 (2011) 4980–4985.
- [11] S. Zhang, W.T. Wu, M.C. Wang, H.C. Man, In-situ synthesis and wear performance of TiC particle reinforced composite coating on alloy Ti6Al4V, *Surf. Coating. Technol.* 138 (2001) 95–100.
- [12] A. Monfared, A.H. Kokabi, S. Asgari, Microstructural studies and wear assessments of Ti/TiC surface composite coatings on commercial pure Ti produced by titanium cored wires and TIG process, *Mater. Chem. Phys.* 137 (2013) 959–966.
- [13] Q.H. Li, M.M. Savalani, Q.M. Zhang, L. Huo, High temperature wear characteristics of TiC composite coatings formed by laser cladding with CNT additives, *Surf. Coating. Technol.* 239 (2014) 206–211.
- [14] M. Xia, A. Liu, Z. Hou, N. Li, Z. Chen, H. Ding, Microstructure growth behavior and its evolution mechanism during laser additive manufacture of in-situ reinforced (TiB+TiC)/Ti composite, *J. Alloys Compd.* 728 (2017) 436–444.
- [15] R. Yang, Z. Liu, G. Yang, Y. Wang, Study of in-situ synthesis TiCp/Ti composite coating on alloy Ti6Al4 V by TIG cladding, *Procedia Eng.* 36 (2012) 349–354.
- [16] G. Rasool, S. Mridha, M.M. Stack, Mapping wear mechanisms of TiC/Ti composite coatings, *Wear* 328 (2015) 498–508.
- [17] J.J. Candel, V. Amigó, J.A. Ramos, D. Busquets, Sliding wear resistance of TiCp reinforced titanium composite coating produced by laser cladding, *Surf. Coating. Technol.* 204 (2010) 3161–3166.
- [18] M.M. Savalani, C.C. Ng, Q.H. Li, H.C. Man, In situ formation of titanium carbide using titanium and carbon-nanotube powders by laser cladding, *Appl. Surf. Sci.* 258 (2012) 3173–3177.
- [19] R. Zhang, Z. Lin, Z. Cui, Q. Song, Studies on multilayer wear of CVD TiC-TiN multilayer composite coating, *Wear* 147 (1991) 227–251.
- [20] Y. Zhu, W. Wang, X. Jia, T. Akasaka, S. Liao, F. Watari, Deposition of TiC film on titanium for abrasion resistant implant material by ion-enhanced triode plasma CVD, *Appl. Surf. Sci.* 262 (2012) 156–158.

- [21] N. Zhao, Y. Xu, J. Wang, L. Zhong, V.E. Ovcharenko, X. Cai, Microstructure and kinetics study on tantalum carbide coating produced on gray cast iron in situ, *Surf. Coating. Technol.* 286 (2016) 347–353.
- [22] I.W. Chen, X.H. Wang, Sintering dense nanocrystalline ceramics without final-stage grain growth, *Nature* 404 (2000) 168–171.
- [23] D. Casellas, J. Caro, S. Molas, J.M. Prado, I. Valls, Fracture toughness of carbides in tool steels evaluated by nanoindentation, *Acta Mater.* 55 (2007) 4277–4286.
- [24] K. Song, Y. Xu, N. Zhao, L. Zhong, Z. Shang, L. Shen, J. Wang, Evaluation of fracture toughness of tantalum carbide ceramic layer: a Vickers indentation method, *J. Mater. Eng. Perform.* 25 (2016) 3057–3064.
- [25] L. Zhong, Y. Xu, M. Hojamberdiev, J. Wang, J. Wang, In situ fabrication of titanium carbide particulates-reinforced iron matrix composites, *Mater. Des.* 32 (2011) 3790–3795.
- [26] P. Ramaekers, F. Vanloo, G. Bastin, R. Metselaar, The use of ternary phase diagram sections in solid-state reactions involving TiC formation, *Solid State Ionics* 16 (1985) 179–184.
- [27] P. Ramaekers, L.V. Fij, G.F. Bastin, Phase relations, diffusion paths and kinetics in the system Fe–Ti–C at 1273 K, *Z. Metallkunde* 76 (1985) 245–248.
- [28] A. Miriyev, M. Sinder, N. Frage, Thermal stability and growth kinetics of the interfacial TiC layer in the Ti alloy/carbon steel system, *Acta Mater.* 75 (2014) 348–355.
- [29] D.R. Ye, J.H. Hu, *Hand Book of Thermodynamics Data for in Organic Substance*, Metallurgy Industry Press, Beijing, 2002.
- [30] H. Zhu, K. Dong, H. Wang, J. Huang, J. Li, Z. Xie, Reaction mechanisms of the TiC/Fe composite fabricated by exothermic dispersion from Fe–Ti–C element system, *Powder Technol.* 246 (2013) 456–461.
- [31] X. Liu, H. Wang, D. Li, Y. Wu, Study on kinetics of carbide coating growth by thermal diffusion process, *Surf. Coating. Technol.* 201 (2006) 2414–2418.
- [32] H. Xu, C. Liu, V.V. Silberschmidt, S.S. Pramana, T.J. White, Z. Chen, V.L. Acoff, Behavior of aluminum oxide, intermetallics and voids in Cu–Al wire bonds, *Acta Mater.* 59 (2011) 5661–5673.
- [33] M.X. Zhang, Q.D. Hu, B. Huang, Study of formation behavior of TiC in the Fe–Ti–C system during combustion synthesis, *Int. J. Refract. Metals Hard Mater.* 31 (2012) 230–235.
- [34] J. Nie, Y. Wu, P. Li, H. Li, X. Liu, Morphological evolution of TiC from octahedron to cube induced by elemental nickel, *CrystEngComm* 14 (2012) 2213–2221.
- [35] D.E. Grove, U. Gupta, A.W. Castleman, Effect of carbon concentration on changing the morphology of titanium carbide nanoparticles from cubic to cuboctahedron, *ACS Nano* 4 (2010) 49–54.
- [36] B. Vishwanadh, K.V.M. Krishna, A. Upadhyay, R. Banerjee, A. Arya, R. Tewari, H.L. Fraser, G.K. Dey, Formation mechanism of the Nb 2 C phase in the Nb–1Zr–0.1C (wt.%) alloy and interrelation between \tilde{a} , \tilde{a} and \tilde{a} -Nb 2 C carbide phases, *Acta Mater.* 108 (2016) 186–196.
- [37] R.O. Ritchie, Mechanisms of fatigue crack propagation in metals, ceramics and composites: role of crack tip shielding, *Mater. Sci. Eng. A* 103 (1988) 15–28.
- [38] A.G. Evans, Perspective on the development of high-toughness ceramics, *J. Am. Ceram. Soc.* 73 (1990) 187–206.
- [39] R.O. Ritchie, The conflicts between strength and toughness, *Nat. Mater.* 10 (2011) 817–822.
- [40] M. Masanta, S.M. Shariff, A. Roy Choudhury, Evaluation of modulus of elasticity, nano-hardness and fracture toughness of TiB₂–TiC–Al₂O₃ composite coating developed by SHS and laser cladding, *Mater. Sci. Eng. A* 528 (2011) 5327–5335.
- [41] S.C. Jambagi, Scratch adhesion strength of plasma sprayed carbon nanotube reinforced ceramic coatings, *J. Alloys Compd.* 728 (2017) 126–137.
- [42] Z. Zhao, P. Hui, T. Wang, X. Wang, Y. Xu, L. Zhong, M. Zhao, New strategy to grow TiC coatings on titanium alloy: contact solid carburization by cast iron, *J. Alloys Compd.* 745 (2018) 637–643.